Geomechanical Modeling of In-Situ Stresses Around a Borehole

Samantha Grandi, Rama Rao, and M. Nafi Toksöz
Earth Resources Laboratory
Dept. of Earth, Atmospheric, and Planetary Sciences
Massachusetts Institute of Technology
Cambridge, MA 02139

Abstract

In this paper, we present a modelling of the in-situ stress state associated with the severe hole enlargement of a wellbore.

Geomechanical information is relevant to assure wellbore stability, i.e., to prevent damages in the formation and later on, the casing. Many of the drilling parameters, as mud weight or the optimal orientation of the borehole, require some knowledge of the mechanical behaviour of the rock. The lack of these kind of data in exploratory areas, where there are usually insufficient constraints for the geological model, increases even more the risk, hence the costs.

The present model uses the concepts of poroelasticity theory to compute the stationary 2D, brittle response of the formation around a borehole that is submitted to effective compressive horizontal stresses. The numerical solution is obtained using a finite element approximation.

The initial stress state at the far field was estimated combining a frictional-failure theory with the observations of dipmeter caliper in a particular borehole that presents elongations in a preferential direction.

The direction and relative extension of the observed breakouts at a particular depth are modelled successfully using formation realistic parameters and dimensions, although the exact shape of the borehole (at all angles) was unknown. For the particular case study, the orientation of the breakout is NE-SW, at about 82 degrees azimuth. Therefore, the maximum horizontal stress lies at approximately 350 degrees azimuth. The ratios of horizontal principal stresses to vertical stress that best honor the observations are $SHmax = 2.3Sv$ and $Shmin = 1.7Sv$. The compressive strength necessary for the rock to fail, as indicated by the caliper data under this stress field, is about 140 MPa.

1 Introduction

In this paper, we present a numerical modelling of the geomechanical conditions of a wellbore where an heterogeneous stress field is responsible for numerous breakouts.

The governing equations are the equations of motion (Navier's equations) for perfectly elastic materials, therefore, only a brittle behavior is assumed and no plasticity is included. A numerical solution computed using the finite element method is presented below. The modelling carried out is a mechanical one and thermal stresses are disregarded. The displacements are assumed invariables with time.

To have the ability of predicting the geomechanical behaviour of the column rock that is to be drillled is a dream-like scenario for the oil industry. In exploration, it is specially relevant, because the uncertainties of the area difficult the selection of drilling parameters as mud weigth, liners depths and so forth.

The issue of wellbore stability has gained particular importance in the last 10 years as a response to the increasing of exploration of complex areas which represent major engineering challenges in drilling and production (Charlez and Onaisi, 2001). Severe hole enlargement has a long list of consequences, from reducing the drill bit life to causing cleaning hole problems, stuck pipe, poor cementing, logging problems, and often the need to sidetrack (Last, 2001).

There are several problems in engineering to which wellbore stability refers. The one addressed in this project, is related to drilling performance where instability is mainly driven by stress concentrations around the cavity.

During drawdown, depletion of fluid could alter pressures significantly. Sometimes, and very much associated with the kind of lithology supporting the reservoir, the casing could suffer important damage and even the total loss of the wellbore (Frederick *et al.*, 1998). A third problem considered as wellbore instability, is sanding production in the completion stage.

During drilling, there are other sources which can also contribute to the development of stability problems. In particular, the orientation of the well has great relevance. Selecting a drilling orientation that does not agree with the natural weak orientation of the formation could introduce difficulties that translate in time and money. On the other hand, there are some laboratory experiments that indicate the damaging effect of some mud components reactions (Charlez and Onaisi, 2001), however, these could only be responsible for washouts of uniform-radius occurrence and not for breakout areas with preferential direction.

There are well established methods to derive the in-situ stress state in a borehole. Among them, breakout analysis, hydraulic fracturing experiments and earthquake focal plane mechanisms, are of wide used (Zoback, 1989). Barton and Zoback (1988) described another stress measurement technique based on stress-induced polarization of tube waves (Stoneley). Sinha *et al.* (1994) introduced a method that uses the flexural mode recorded in cross-dipole data to distinguish induced stresses in the borehole. Finally, the resolution improvement of borehole imaging logs, have made the in-situ stress derivation another application of this tool, overcoming the limitation of four-arms caliper data to provide all-azimuth measurements (Brudy and Kjorholt, 2000).

Each method has its own limitations. In all of these techniques (with the exception of focal mechanisms), the stress state inverted includes the effects of any drill-induced stress in the wellbore superimposed to the tectonic field. If the formation is anisotropic, the stress anisotropy would amplify or alter by the presence of the bore (Zoback, 1989), being these effects sometimes larger than the in-situ stresses existing before drilling the well. Knowledge of the ambient stress field is important in elucidating tectonic processes.

To understand the behaviour of a wellbore in a tectonically pre-stressed region, forward modelling is a necessary procedure. In this project we are willing to quantify the tectonic stress effect in the formation around a well that does not present any significant anisotropy, at least at the depth of study. However, the heterogeneties of the far field stresses are responsible for important geomechanical damages.

The paper is structured in the following way: first, a background theory is presented to facilitate the description of the numerical modelling. Second, the problem is described along with the derivation of the model parameters. Finally, the results are presented and discussed. In brief, the formation parameters are computed from the well data available and the initial range of values of the principal stresses is obtained by a standard analysis of breakouts inferred from the dipmeter caliper data.

2 Theoretical Background

2.1 Structural Mechanics

When a layer of rock, buried at certain depth, is submitted to a stress field, the displacements and displacement gradients are sufficiently small for the theory of linear elasticity to be valid. The equations of motion, or equilibrium, can be considered to be satisfied in the undeformed reference configuration. We chose the Lagrangian description of motion to express the global conservation laws. Because of the fixed material viewpoint, the conservation of mass is automatically satisfied.

Using conservation of momentum, the Cauchy's equations of motion are obtained (Malvern, 1969). In vectorial notation,

$$\nabla T + f = \rho \frac{\partial u}{\partial t}, \tag{1}$$

where u is the velocity, ρ is the density of the material, f represents the body forces per unit volume and T is the stress tensor defined as:

$$T = \begin{bmatrix} \sigma_x & \tau_{xy} & \tau_{zx} \\ \tau_{xy} & \sigma_y & \tau_{yz} \\ \tau_{zx} & \tau_{yz} & \sigma_z \end{bmatrix} \tag{2}$$

σ_i represent the normal stresses and τ_{ij} the shear stresses.

In the special case of static equilibrium, the acceleration $\frac{\partial u}{\partial t}$ is zero and equation (1) reduces to:

$$\nabla T + f = 0 \tag{3}$$

In general, $T_{ij} = T_{ji}$, and there are only six independent unknown stress components instead of nine. However, the 3 equations (1) are still not enough to solve for the stresses, and constitutive equations have to be used. The stress-strain relations describe the ideal macroscopic behavior of the material under consideration. For an ideal elastic solid, the constitutive equations are known as Hooke's law :

$$T = C\epsilon, \tag{4}$$

where C is a fourth-rank tensor with 36 independent coefficients (in the most general case), and ϵ is the strain tensor

$$\epsilon = \begin{bmatrix} \epsilon_x & \gamma_{xy} & \gamma_{zx} \\ \gamma_{xy} & \epsilon_y & \gamma_{yz} \\ \gamma_{zx} & \gamma_{yz} & \epsilon_z \end{bmatrix} \tag{5}$$

By definition, the strains are related to the displacements, $\bar{u}$ = (u,v,w), as:

$$\begin{aligned} \epsilon_x &= \frac{\partial u}{\partial x}; & \epsilon_{xy} &= \frac{\gamma_{xy}}{2} = \frac{1}{2}\left(\frac{\partial u}{\partial y} + \frac{\partial v}{\partial x}\right) \\ \epsilon_y &= \frac{\partial v}{\partial y}; & \epsilon_{yz} &= \frac{\gamma_{yz}}{2} = \frac{1}{2}\left(\frac{\partial v}{\partial z} + \frac{\partial w}{\partial y}\right) \\ \epsilon_z &= \frac{\partial w}{\partial z}; & \epsilon_{zx} &= \frac{\gamma_{zx}}{2} = \frac{1}{2}\left(\frac{\partial w}{\partial x} + \frac{\partial u}{\partial z}\right) \end{aligned} \tag{6}$$

For an elastically isotropic material, the coefficients of C can be expressed in terms of only two elastic modulii. Usually, these are either the Lame constants, λ and μ, the Young's modulus (E) and Poisson ratio ν, or the bulk modulus K and the shear modulus (G). The bulk modulus is a measure of the fractional volume change when the pressure is increased by δP. It is obtained through isotropic compression experiments. Most frequently, uniaxial compression is simpler to perform, in which case, it is the Young's modulus that it is measured. By definition,

$$E = \frac{\sigma_{zz}}{\epsilon_{zz}} \tag{7}$$

On the other hand, the deformations that take place in the transversal direction are described by the Poisson ratio:

$$\nu = -\frac{\epsilon_{yy}}{\epsilon_{zz}} \tag{8}$$

(Gueguen, 1994).

Using the Young's modulus (E), and the Poisson's ration (ν), Hooke's law reduces to:

$$\begin{aligned} \sigma_x &= \frac{E}{1+\nu}\left(\epsilon_x + \frac{\nu}{1-2\nu}(\epsilon_x + \epsilon_y + \epsilon_z)\right); & \tau_{xy} &= G\gamma_{xy} \\ \sigma_y &= \frac{E}{1+\nu}\left(\epsilon_y + \frac{\nu}{1-2\nu}(\epsilon_x + \epsilon_y + \epsilon_z)\right); & \tau_{yz} &= G\gamma_{yz} \\ \sigma_z &= \frac{E}{1+\nu}\left(\epsilon_z + \frac{\nu}{1-2\nu}(\epsilon_x + \epsilon_y + \epsilon_z)\right); & \tau_{zx} &= G\gamma_{zx} \end{aligned} \tag{9}$$

where G is defined as:

$$G = \frac{E}{2(1+\nu)} \tag{10}$$

Finally, substituting equation (6) in (9) and equation (9) in (3), Navier's displacement equations of motion are:

$$-\nabla C \nabla u = f, \tag{11}$$

where,

$$C = \begin{bmatrix} \begin{bmatrix} 2G+\mu & 0 & 0 \\ 0 & G & 0 \\ 0 & 0 & G \end{bmatrix} & \begin{bmatrix} 0 & \mu & 0 \\ G & 0 & 0 \\ 0 & 0 & 0 \end{bmatrix} & \begin{bmatrix} 0 & 0 & \mu \\ 0 & 0 & 0 \\ G & 0 & 0 \end{bmatrix} \\ \begin{bmatrix} 0 & G & 0 \\ \mu & 0 & 0 \\ 0 & 0 & 0 \end{bmatrix} & \begin{bmatrix} G & 0 & 0 \\ 0 & 2G+\mu & 0 \\ 0 & 0 & G \end{bmatrix} & \begin{bmatrix} 0 & 0 & 0 \\ 0 & 0 & \mu \\ 0 & G & 0 \end{bmatrix} \\ \begin{bmatrix} 0 & 0 & G \\ 0 & 0 & 0 \\ \mu & 0 & 0 \end{bmatrix} & \begin{bmatrix} 0 & 0 & 0 \\ 0 & 0 & G \\ 0 & \mu & 0 \end{bmatrix} & \begin{bmatrix} G & 0 & 0 \\ 0 & G & 0 \\ 0 & 0 & 2G+\mu \end{bmatrix} \end{bmatrix} \tag{12}$$

and $\mu = \frac{E\nu}{(1+\nu)(1-2\nu)}$ Once the derivatives of the displacements have been obtained, all strain and stress components can be derived.

In modelling the deformations around the borehole, plane strain is an appropriate 2D approximation since we can assume no displacements take place in the z-direction (borehole axis) and the displacements in x and y directions are functions of x and y but not z (Malvern, 1969). Then, $\epsilon_z = \gamma_{yz} = \gamma_{zx} = 0$ and in eq.(11) u = (u,v) and :

$$C = \begin{bmatrix} \begin{bmatrix} 2G+\mu & 0 \\ 0 & G \end{bmatrix} & \begin{bmatrix} 0 & \mu \\ G & 0 \end{bmatrix} \\ \begin{bmatrix} 0 & G \\ \mu & 0 \end{bmatrix} & \begin{bmatrix} G & 0 \\ 0 & 2G+\mu \end{bmatrix} \end{bmatrix} \tag{13}$$

2.2 Stress State in the Earth

To describe the stress field completely in the Earth we need only to refer to the orientation and magnitudes of the principal stresses. The principal stresses are the normal stresses that act on planes oriented such that shear stresses vanish. For simplicity we will refer to those stresses as S1, S2 and S3:

$$\begin{aligned} S1 &= (\lambda+2G)\epsilon_1 + \lambda\epsilon_2 + \lambda\epsilon_3 \\ S2 &= \lambda\epsilon_1 + (\lambda+2G)\epsilon_2 + \lambda\epsilon_3 \\ S3 &= \lambda\epsilon_1 + \lambda\epsilon_2 + (\lambda+2G)\epsilon_3 \end{aligned} \tag{14}$$

where λ = (E ν)/(1 - 2 ν)(1 + ν).

Within the lithosphere, the principal planes appear to be oriented approximately horizontally and vertically (Zoback, 1989). In general, $SHmax$ describes the maximum principal horizontal stress and $Shmin$, the minimun principal horizontal stress. Furthermore, the principal stress that is essentially vertical, Sv, can be described as the stress induced by the weight of the overlying rock

$$Sv \sim \int \rho(z) g \, dz \tag{15}$$

where ρ(z) is the density of the overlying rock, g is the gravitational constant and z is the depth. For an average density of 2.5 g/cm^3, the change in vertical stress with depth is approximately 25 Mpa/km, (Zoback, 1989).

From faulting theory, first elaborated by E.M. Anderson (Anderson, 1951), it can be shown that in areas of extension, $Sv \geq SHmax \geq Shmin$; in areas of strike slip faulting $SHmax \geq Sv \geq Shmin$; and in areas of reverse faulting $SHmax \geq Shmin \geq Sv$. Thus, the relative magnitudes of the three principal stresses defines the tectonic style and, as Sv at depth can be estimated from average rock density, it provides a convenient reference respect to which the horizontal principal stresses can be estimated.

2.3 Generalization to Poroelasticity

The magnitudes of the principal stresses at depth are affected by the presence of fluids in cracks and pores in the rocks. The description of small deformations of saturated porous medium, requires the use of poroelasticity theory.

Elastic modulii, rock strength and frictional strength, depend on the effective stress,

$$\sigma_{ij} = T_{ij} - \delta_{ij}\alpha P_p \tag{16}$$

where σ_{ij} now represent the effective stresses, T_{ij} are the components of the stress matrix as before, P_p is the pore pressure, δ_{ij} is the Kronecker delta and α is the Biot constant defined as: $\alpha = 1 - (K_b/K_g)$ (Gueguen, 1994). K_b is the drained bulk modulus of the porous rock and K_g is bulk modulus of the solid grains. $\alpha = 0$ implies that the rock has almost no pores while $\alpha = 1$ would correspond to an extremely compliant porous solid. As noted in equation (16), pore pressure reduces the effects of total stress at depth.

For an ideal poroelastic material, the constitutive relations are linear as in elasticity. The stress-strain relations, disregarding isothermal effects, will depend on the deformation regime considered, that is, drained, where the fluid pressure is constant, or undrained where the fluid pressure is variable. In the drained regime, the governing equations of linear elasticity still hold if the stresses, strains and elastic modulii are replaced by their effective counterparts:

$$\epsilon_{ij} = \frac{1}{2G}(T_{ij} - \delta_{ij}T_{00}) + \frac{1}{3K}\delta_{ij}T_{00} - \frac{\alpha}{3K}\delta_{ij}P_p \tag{17}$$

where $T_{00} = \frac{1}{3}(T_{11} + T_{22} + T_{33})$ is the uniform confining pressure. From eq.(17), if only shear deformations are involved, $\epsilon_{ij} = T_{ij}/2G$ $(i \neq j)$, showing that shear stresses (and strains) are not affected by P_p.

2.4 Stress State Around the Wellbore

The equations describing the concentration of stresses in a plate with a circular hole under uniform tension at infinity, were first derived by G.Kirsch in 1898 (Malvern, 1969). By modifying these equations to include effective minimum and maximum compressive stresses and the fluid pressure in the hole, the description of a cylindrical hole in a homogeneous, isotropic elastic plate can be generalized. Disregarding any thermal stresses:

$$\begin{aligned}
\sigma_r &= \frac{1}{2}(SH^* + Sh^*)(1 - \frac{R^2}{r^2}) + \frac{1}{2}(SH^* - Sh^*)(1 - 4\frac{R^2}{r^2} + 3\frac{R^4}{r^4})\cos(2\theta) + \frac{\Delta P R^2}{r^2} \\
\sigma_\theta &= \frac{1}{2}(SH^* + Sh^*)(1 + \frac{R^2}{r^2}) - \frac{1}{2}(SH^* - Sh^*)(1 + 3\frac{R^4}{r^4})\cos(2\theta) - \frac{\Delta P R^2}{r^2} \\
\tau_{r\theta} &= -\frac{1}{2}(SH^* + Sh^*)(1 + \frac{2R^2}{r^2} - 3\frac{R^4}{r^4})\sin(2\theta)
\end{aligned} \tag{18}$$

(Jaeger, 1979), where σ_r is the radial stress, σ_θ is the circumferential stress, $\tau_{r\theta}$ is the tangential shear stress, R is the radius of the hole, θ is the azimuth measured from the direction of SH^* and ΔP is the difference between the fluid pressure in the borehole and that in the formation (positive indicates excess pressure in the borehole); SH^* and Sh^* refer to the effective horizontal principal stresses, $(S^* = S - P_p)$.

Anderson's faulting theory predicts stress magnitudes at depth through the utilization of simplified two-dimensional Mohr-Coulomb circles. The also known as Coulomb-Navier failure criterion in frictional equilibrium, assumes that failure is only a function of the difference between the least and the greatest principal stresses $S1$ and $S3$:

$$\frac{S1 - P_p}{S3 - P_p} = [(\mu^2 + 1)^{1/2} + \mu]^2 \tag{19}$$

where μ is the coefficient of friction, that varies in most rocks between 0.6 and 1.0 (Byerlee, 1978). If there is a preexisting fault plane, frictional sliding will occur when the ratio of shear stress to effective normal stress is equal to the coefficient of friction of the rock (Jaeger, 1979).

Following Anderson's theory, equation (19), allows to define the limiting stress magnitudes for different tectonic environments: in extensional areas $Shmin \simeq 0.6Sv$, in reverse faulting areas $SHmax \simeq 2.3Sv$ and in strike slip faulting areas if $Sv \simeq 1/2(SHmax + Shmin)$, $SHmax \simeq 2.2Shmin$ (Zoback, 1989).

For a reverse faulting case, figure 1 shows the variation of hoop stress as a function of azimuth for different nominal values of $SHmax$ and $Shmin$. Hoop stress is described by equations (18) when $r = R$. In figure 1, ΔP = -0.98MPa and a hydrostatic gradient for the pore pressure was assumed (Pp = 27.8 MPa).

Hoop stresses are maximum at 90° and minimun at 0°:

$$\sigma_{0^\circ} = 3SHmax - Shmin - 2P_p - \Delta P$$
$$\sigma_{90^\circ} = 3Shmin - SHmax - 2P_p - \Delta P \tag{20}$$

In general, failure will occur when the strength of the rock is exceeded by the concentrated stress. For instance, if the rock had a strength $C_0 = 150$ Mpa, as shown in figure 1, the failure around the borehole would be restricted to the angle range $\theta = -40^\circ$ to -90° when $SHmax = 2.3Sv$ and $Shmin = Sv$. To not have any failures under this stress field, the rock has to have a compressive strength larger than 300 MPa. On the contrary, if it is as weak as 40 MPa, it will fail at all azimuths. In general, compressive strength is inversely related to porosity. The function σ_θ steepens as the difference between $SHmax$ and $Shmin$ is larger.

The former concepts will be used in the next sections to understand the initiation of breakouts in a particular well case.

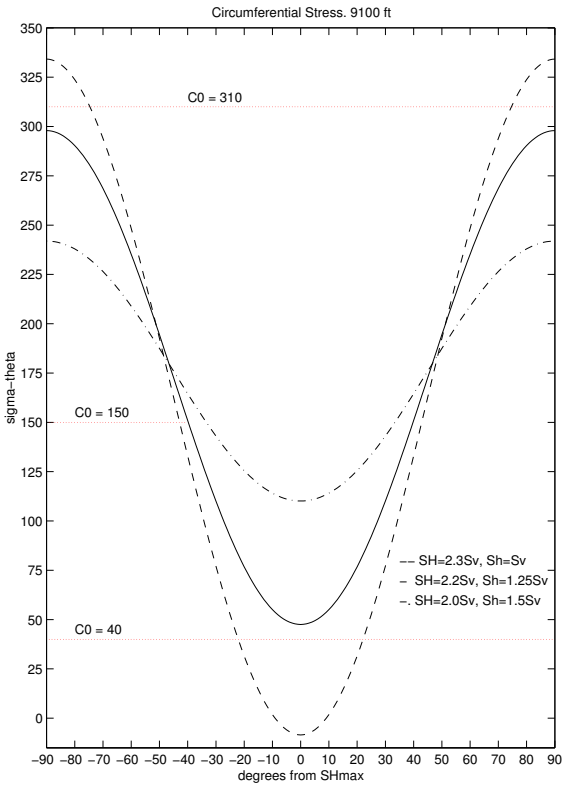

Figure 1: Hoop Stress as described by eq. (18) when r = R, Pp = 27.8 MPa and ΔP = -0.98 MPa. Sv at 9100 ft is 65.9 MPa

3 Well Description and Model Parameters

The well of study, hereinafter referred as well M, is a wild-cat drilled in an exploratory area known to be tectonically complex, where reverse faulting is the structure-controlling regime expected. The data available corresponded to the depth interval 4500 to 12989 ft and in fig. 2 some logs are plotted.

As shown in fig.2, two caliper measurements (C1-4 and C2-3) were available as recorded by the dipmeter tool. The dipmeter is mainly logged to measure the structural dip of bedding planes intersecting the well. In the case of well M, the tool used has four pad-type micoinduction sensors, arranged in an orthogonal pattern,

that measure the variation of formation conductivity. The reference pad, pad 1, is magnetically oriented and two independent calipers measure the borehole diameter between pads 1-3 and 2-4. The four-arm dipmeter aligns with the long axis of a noncircular borehole.

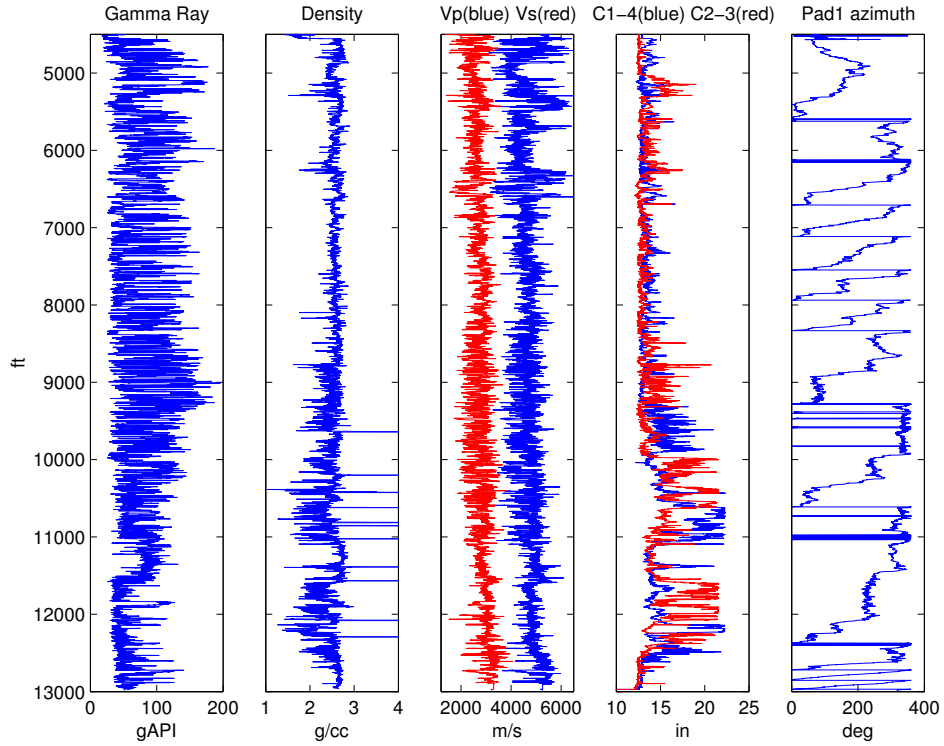

Figure 2: Some logs from well M

Plumb and Hickman (1985), based on a comparison between the dipmeter-derived borehole elongations and those determined independently from the borehole televiewer tool, concluded that the former can be used reliably to infer directions of $Shmin$.

From the caliper data, it is clear that the borehole has undergone significant failure below 8500 ft. In some cases as in 10400 ft, the hole diameter reaches 22.3 inches, almost the double of the bit size (12.25 in). If there is no systematic relationship between the orientation of these borehole elongations with either the deviation of the well[1] or natural fractures intersecting the well, they must be associated to the stress concentration. The purpose of the following modelling is precisely to obtain the stress state responsible for this deformation.

Acoustic logs, specifically, cross-dipole data were analysed to rule out the presence of drilling-induced stress in the wellbore. Since it is not the issue of this paper, only the dispersion curves at 9100 ft are shown in fig.3. The ellipticity of the borehole at this depth requires the dispersion curves to be corrected by the borehole size. Apparent anisotropy is eliminated after this correction and an isotropic behaviour of the formation at this depth around the well can be assumed. Thus, any estimation of in-situ stresses will be most likely associated with a tectonic origin.

For the purposes of the following modelling, some formation parameters as well as an initial estimation of the far field stresses have to be specified.

Due to the absence of laboratory data, Young modulus and Poisson ratio were derived from the velocities

[1]Well M can be considered vertical since the maximum deviation is approx. 4°

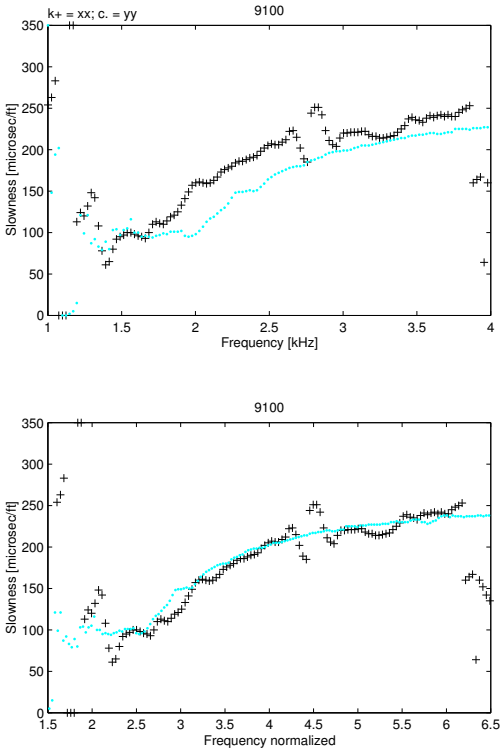

Figure 3: Dispersion curves of flexural wave recorded with cross dipole log. Blue (.) corresponds to source and receiver in x-dir and black (+) to y-dir. A separation of these curves would imply anisotropy in the near field (upper figure). Frequency was normalized by borehole size in both directions in the lower figure where now the behaviour is isotropic.

of P (V_p) and S (V_s) waves, recorded in monopole sonic data (fig. 2),

$$E = \rho V_s^2 \frac{3V_p^2 - 4V_s^2}{V_p^2 - V_s^2} \quad (21)$$

$$\nu = \frac{V_p^2 - 2V_s^2}{2(V_p^2 - V_s^2)} \quad (22)$$

The variation of pore pressure with depth to get the effective stresses is usually estimated from the sonic porosity, the resistivity data or even seismic data. In this case, a hydrostatic gradient was assumed (10 Mpa/km) (Zoback, 1989).

The vertical principal stress Sv is computed by integrating the density log (equation 15). Substracting the pore pressure, the effective vertical stress is obtained. Sv is plotted in figure 4 along with a lithostatic gradient of 25MPa/km.

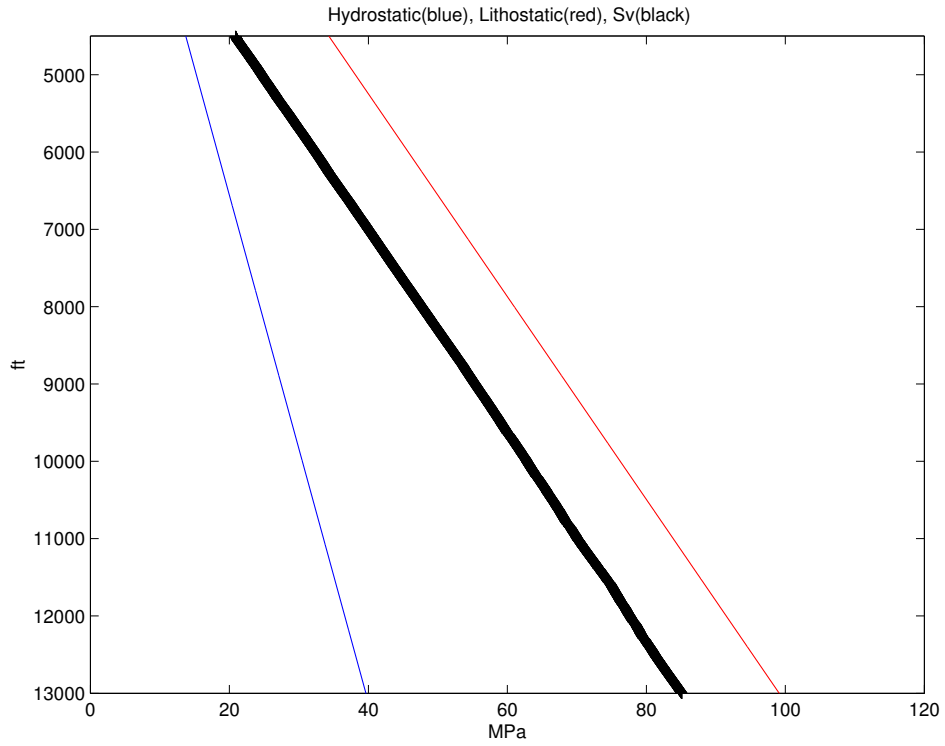

Figure 4: Variation of Sv and hydrostatic pressure with depth. Sv was derived from the density log

4 Initial Estimation of Horizontal Stresses

When a borehole is drilled, the stresses that were previously supported by the material that was exhumed are transferred to the surrounding material. There are basically two direct ways in which the stress concentrations around boreholes can be used to obtain in-situ stresses.

The first method, known as hydraulic fracturing involves inducing a tensile fracture at the point where the concentrated hoop stress is least compressive, that is at the azimuth of $SHmax$ (Zoback, 1989). Above 3 km where pressures and temperatures are below the limit of commercially available equipment, hydraulic fracturing experiments can be carried out (Zoback *et al.*, 1986).

The second method occurs naturally in many boreholes because the compressive hoop stress around a hole can be large enough to exceed the strength of the rock. When this happens, the rock around a portion of

the wellbore fails and stress-induced wellbore breakouts form. Breakouts develop at the azimuth of $Shmin$, that is, the hole elongates perpendicular to the maximum compressive stress (eqs. 18). Breakouts are more likely at greater depths because although rocks tend to be stronger, stresses increase with depth.

By observing the caliper data of well M (fig. 2), three possible behaviours can be distinguished:

(1) Where breakouts do not occur or occur very slightly, as above 8500 ft and below 12600 ft.

(2) Where breakouts occur only at one point, the region of maximum compressive stress concentration (A), as between 9000 and 10000 ft. and between 11600 and 12500 ft.

(3) Where they occur at point A and B (region parallel to $SHmax$), although more pronounced at point A (10000-11000 ft).

Note that there is no systematic relationship between these areas and depth. That a borehole can breakout at all angles or in a particular range depends only on the magnitude of the stresses relative to the strength of the rock.

Utilization of denser drilling fluids helps to prevent breakout formation. This practice, however, slows the operation and has several other drawbacks. In any case, the extension of breakouts in well M are so large that probably they couldn't have been completely avoided even if mud had been heavier. Assuming a hydrostatic pore pressure, there is (in average) a slight underbalance at the depth interval of study (ΔP = -0.99 MPa).

In order to explain the damages in well M, the modelling was done to approximate the observations at 9100 ft, a depth where the borehole has deformed in one preferential direction. The data at 9100 ft. is summarized in table 1.

Table 1: Formation parameters at 9100 ft. C1 and C2 refer to caliper between pad 1 and 4 and between pad 2 and 3 respectively. P1AZ is the azimuth at pad 1

Gamma Ray	55.2 gAPI
Density	2.422 g/cm^3
Vp	4774 m/s
Vs	3067 m/s
Porosity	8 %
C1	15.2988 in
C2	12.3705 in
P1AZ	82.22 deg
E	52 GPa
ν	0.1486
Hydrostatic Pp	27.8 MPa
Mud Density	0.985 g/cm^3
Mud weight	26.82 MPa
ΔP	-0.98 MPa

The direction of the principal stresses can be reliably inferred from the breakout occurences, but how can the magnitudes be estimated? We followed an standard procedure in breakout analysis (Barton *et al.*, 1988).

First we use Anderson's theory and equation (19) to define the limiting stress magnitudes in the $SHmax$, $Shmin$ space assuming a coefficient of friction of 0.6. Second, we obtain a range of possible values of rock strength (C_0) based on the observation that at 9100 ft. breakouts only occur at point A and not at B. Finally, we superpose both informations to get the possible stresses in the area of overlap.

Usually, when measurements of C_0 are available from core samples, the procedure outlined before gives a well constrained region of possible values of stresses. In this case, the strength of the rock is unknown, however, several facts can be used to limit the possible range of values of C_0:

1.) In figure 1, it can be observed that the curve that spans the largest range of possible C_0 is when $SHmax = 2.3Sv$ and $Shmin = Sv$. This combination represents extreme values since $SHmax$ can not be

larger if frictional equilibrium is assumed. Similarly, $Shmin$ can not be smaller than Sv if the well is in a reverse faulting area. To get compressive failure under this stress state only at point A, would require that the rock compressive strength were not greater than 330 MPa.

2.) The differences between the 3 principal stresses tend to be larger in reverse faulting areas than in normal faulting or strike slip regions (Zoback, 1989); this implies that most probably $Shmin$ will be larger than Sv. Hence, the lower limit of C_0 will also increase. For instance, if $SHmax = 2.3\ Sv$ and $Shmin = 1.6\ Sv$, C_0 should be larger than 125 MPa and weaker than 300 MPa for the rock to fail only at A and not in B.

3.) At 9100 ft. the sonic-derived porosity of the formation is approximately 8%. The gamma ray lecture (55° API) indicates that the rock may be a sandstone. Some laboratory measurements of strength in sandstones of similar porosities report values between 50 a 250 MPa.

The limits of compressive strength range equate the minimum and maximum hoop stresses,

$$\begin{aligned} C_0(\sigma_{90^\circ}) = &\quad 3SHmax - Shmin - P_p - \Delta P \\ C_0(\sigma_{0^\circ}) = &\quad 3Shmin - SHmax - P_p - \Delta P \end{aligned} \tag{23}$$

These two lines define the regions of possible failure occurrence. When superposed to the frictional equilibrium $SHmax - Shmin$ regions, a range of stress values can be defined. Figure 5 shows this region for $C_0 = 200$ MPa and table 2 summarizes the estimations for different values of C_0.

Table 2: Possible range of stresses for nominal C_0 at 9100 ft. Breakouts in A but not in B

case	C_0 [MPa]	$SHmax/Sv$	$Shmin/Sv$
1	250	1.7 - 2.3	1 - 2
2	200	1.4 - 2.3	1- 1.7
3	150	1.1 - 2.3	1- 1.4
4	100	1.5 - 2.3	1 - 1.2

5 Numerical Modelling

The modelling of the in-situ stress state consists in solving the Navier's equations of motion for displacements and getting strain and stress components through Hooke's law. Because only a stationary solution of the Navier's equations is considered, the deformation of the borehole is assumed to happen "instantaneously" after the application of forces. Whether these kind of failures in wellbores are time-dependent or not is not the subject of this paper, however, some observations indicate that the exposure time might be an important factor to explain severe drilling problems (Last, 2001).

The equations were solved numerically using a finite element approximation which is based on the variational formulation of the problem that reduces second order PDE's to first order equations. Once the governing equations are in their weak form, the displacement vector is approximated over the region by finite element interpolations (Reddy, 1993).

FEMLAB[2] was the software used to calculate the numerical solution. The area was meshed using curved triangular elements that refined towards the borewalls (fig. 6). The mesh consisted of 8024 nodes and 15712 elements.

In order to obtain a stable solution, boundary conditions have to be imposed. The outer edges were considered fixed in the direction perpendicular to the stress applied. At the same borders, forces per unit area representing the far field stresses were specified, $SHmax = F_x$ and $Shmin = F_y$, where F_i is the force per unit area in the i direction normal to the boundary: $F_i = \sigma_i \cdot n_i$.

[2]PatentPending. Copyright 1994-2001 Comsol AB

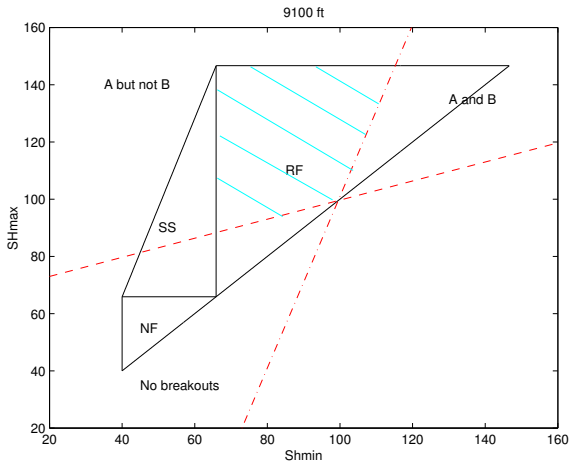

Figure 5: Limits of stress differences from frictional failure theory. NF represents a normal faulting regime where Sv is the largest of the principal stresses. SS indicates strike slip where Sv is the second largest stress. RF represents an area of reverse faulting where Sv is the lowest stress. The red lines indicate the maximum and minimum hoop stress for a compressive strength of 200 MPa. They define three regions: where breakouts do not occur, where they occur at point A only and where they occur at A and B. At 9100 ft, breakout occurs only at point A and the tectonic regime is known to be RF, thus just the region in blue spans the possible values of SHmax and Shmin

The range of horizontal stresses estimated as previously explained was investigated until the concentration of stresses around the borehole was enough to produce the observed deformation at 9100 ft given a particular rock compressive strength.

Force per unit area corresponding to the mud pressure inside the hole, were specified at the boundary of the well bore. This force acts in opposite directions respect to the ones at the outer boundaries of the model, however, it is much smaller (27.8 MPa).

The dimensions of the model were chosen to be realistic. The diameter of the undeformed wellbore coincides with the bit size in well M (12.25 in.). To define how far from the wellbore should the tectonic stresses be specified a simple test was performed. Displacements were computed for different geometries (from as close to the borewall as 0.02 m to 1 m) and a stable solution was observed as the stresses were applied further away from the bore. This indicated that a distance of 1 m. from the borehole wall is enough to be considered as the far field.

6 Results

At 9100 ft the larger diameter of the borehole is at 82 degrees azimuth, indicating that the direction of $SHmax$ should be around 352 degrees azimuth, The methodology applied give us some insigth into the relative magnitudes of the principal stresses.

In fig. 7, the modelling was carried out for far field stresses $SHmax = 2.3Sv$ and $Shmin = 1.2Sv$. It is observed that the maximum concentration of stresses occurs at the azimuth of $Shmin$ (N-S in the figure). This is the region that will undergo compressive failure if the rock is weak enough. Note that there are some tensile stress accumulation at the azimuth of $SHmax$; if the rock at this point had a tensile strength smaller than the values obtained ($T_0 = 70$ MPa), stress induced fractures will form at this azimuth. Usually, tensile strengths are very small and often they are approximated to 0 MPa, however, tensile fractures are not likely to happen in this case since it would require negative values of hoop stresses. These could be yield if using excessive heavy muds (not the case) or when $Shmin$ is smaller than $SHmax$, an invalid condition if in transverse faulting. Furthermore, the formation behaves isotropically at this depth as already shown in fig. 3.

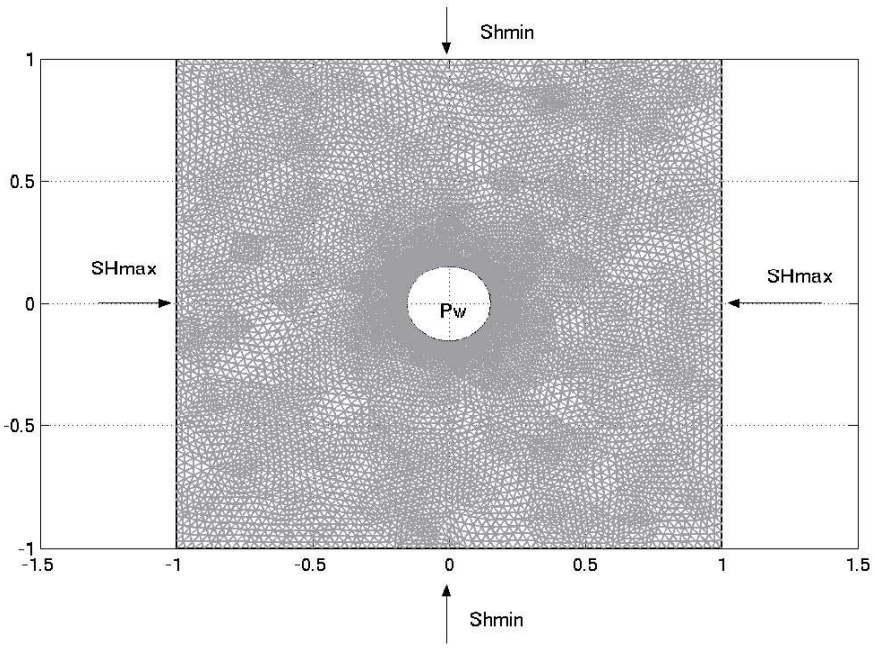

Figure 6: Finite Element Mesh and Boundary Conditions

The previous analysis suggests that initial values of $SHmax$ or $Shmin$ must be different. As mentioned before, $Shmin$ is usually larger than Sv in this regime, therefore, $Shmin$ was increased until tensile stresses practically dissapeared from the solution. Moreover, the well presents breakouts in A and B at other depths being an example at 10400 ft where $Sv = 64.4$ MPa, similar to the value at 9100 ft. Thus, we shouldn't expect much differences between $Shmin$ at both depths, and in order to fail at all azimuths $Shmin$ has to be large enough.

Boundary conditions of $Shmin = 1.7Sv$ and $SHmax = 2.3Sv$ were assumed in fig.8. From it, we can infer that the compressive strength of the rock has to be 140 MPa to produce the observed deformation (about 0.035 m from the original diameter of the hole in both directions). Hoop stresses at the azimuth of $SHmax$ are approximately 15 MPa. As expected, they are not enough to overcome the strength of the rock, hence no failure takes place at B.

From figure 8, tectonic stresses of $SHmax = 2.3Sv$ and $Shmin = 1.7Sv$ are reasonable yet non-unique magnitudes that can explain the observations. No tensile fractures or breakouts are formed at the azimuth of $SHmax$ and expected enlargements of the borehole can occur at the azimuth of $Shmin$, if rock strength is about 140 MPa. Moreover, the width of the breakout in this case may be inferred to be between 340 and 20 deg. azimuth, nevertheless, these results can not be confirmed due to the lack of borehole image logs.

The deformation of the borehole in the y-direction, this is in the region of maximum concentration of compressive stress, is about 0.3 mm. These displacements are two order of magnitudes smaller than the observations. However, the discrepancy was expected provided a linear elastic behaviour was initially assumed; as a consequence, unrealistic high stresses are required to reproduce the actual deformations.

Rocks at these temperatures and confining pressures deform non-elastically and creep constitutive laws describe better the stress-strain relationships. In order to obtain a more accurately quantitative result, the model needs to be time-dependent.

7 Conclusions

The formation of breakouts has been succesfully described by poroelasticity and failure-frictional theory. Further studies on the in-situ stress state are encouraged through the use of forward modelling. However,

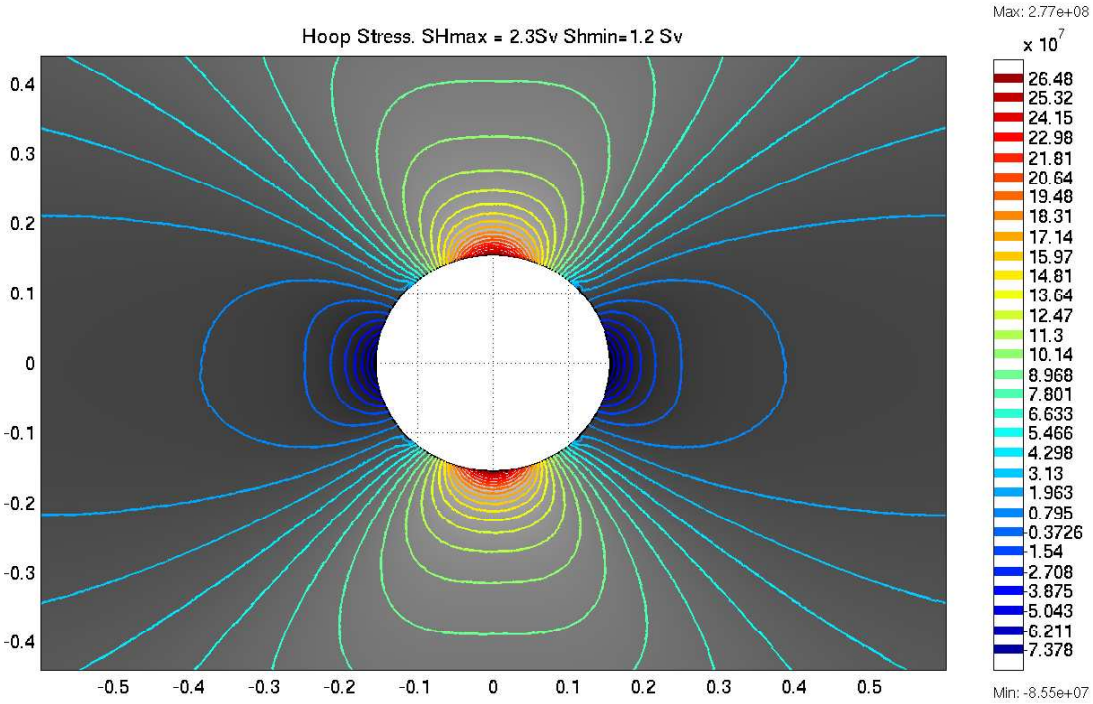

Figure 7: Hoop Stress for initial SHmax = 2.3 Sv and Shmin = 1.2 Sv. Note the negative values at the azimuth of SHmax associated with tensile stresses

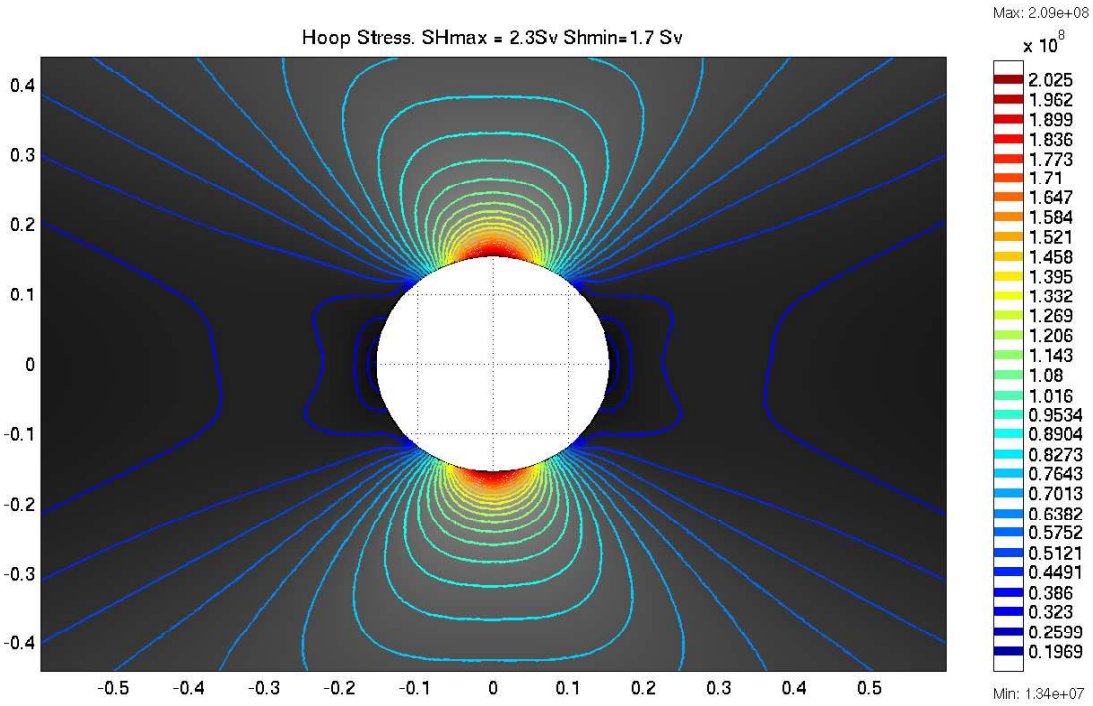

Figure 8: Hoop Stress for initial SHmax = 2.3 Sv and Shmin = 1.7 Sv. The concentration of compressive stresses at the azimuth of SHmax is lower than the compressive strength of the formation therefore, failure only takes place at the azimuth of Shmin

the small deformations inverted suggest that creeping processes should be involved in the formation of the observed failures. The modelling has to be modified to include this non-linear behaviour of the rock.

Significant ellipticity of boreholes requires the incorporation of corrections by the borehole size on the logs processing, in order to avoid erroneous interpretation of anisotropic conditions in the formation around the well.

Caliper data at only two directions is a limitation in characterizing the width of breakouts. Borehole image logs , core information and formation pressure data are required for validating the results here obtained.

8 Acknowledgments

The authors would like to thank PDVSA, Exploration and Production Division, for the permission to publish this paper and for providing the well data.

This work was supported by the Earth Resources Laboratory's Borehole Acoustics and Logging Consortium, and by the Founding Members of the Earth Resources Laboratory at the Massachusetts Institute of Technology.

References

Anderson, E.M, 1951; *The Dynamics of Faulting and Dyke Formation With Applications to Britain*, Ed. Oliver and Boyd, Edimburgh, 2nd Edition

Barton, C.A. and M.D. Zoback, 1988; *Determination of in Situ Stress Orientation From Borehole Guided Waves*, Journal of Geophysical Research, 93(B7), pp 7834-7844

Barton, C.A., M.D. Zoback and K.L. Burns, 1988; *In-Situ Stress Orientation and Magnitude at the Fenton Geothermal Site, New Mexico, determined from Wellbore Breakouts*, Geophysical Research Letters, Vol. 15, No. 5, pp 467-470.

Brudy, M. and H. Kjorholt, 2000; *Stress Orientation on the Norwegian continental shelf derived from borehole failures observed in high-resolution borehole imaging logs*, Tectonophysics, 337, pp 65-84.

Byerlee, J.D., 1978; *Friction on rocks*, Pure Appl. Geophys., 116, pp 615-626.

Charlez, P.S. and A. Onaisi, 2001; *Wellbore Stability: One of the Most Important Engineering Challenges When Drilling Smart Wells*
in Interactive Drilling for fast track Oilfield Development, Ed. J. Lecourtier, TECHNIP, pp 77-102.

Frederick, J., G. Deitrick, J. Arguello and E. de Rouffignac, 1998; *Reservoir Compaction, surface subsidence, and casing damage: a geomechanincs approach to mitigation and reservoir management*, SPE/ISRM EUROCK, #47284.

Gueguen, Y. and V. Palciauskas, 1994; *Introduction to the Physics of Rocks*, Princeton Univ. Press.

Jaeger, J.C. and N.G. Cook, 1979; *Fundamentals of Rock Mechanics*, London: Chapman and Hall.

Last, N.C., 2001; *Achieving and Maintaining Improved Drilling Performance in the Tectonically Stressed Andean Foothills of Colombia*
in Interactive Drilling for fast track Oilfield Development, Ed. J. Lecourtier, TECHNIP, 59-75.

Malvern, L.E., 1969; *Introduction to the Mechanincs of a Continuous Medium*, Prentice-Hall.

Plumb, R.A. and S.H. Hickman, 1985; *Stress-Induced Borehole Elongation: A Comparison Between the Four-Arm Dipmeter and the Borehole Televiewer in the Auburn Geothermal Well*, Journal of Geophysical Research, 90(B7), pp 5513-5521.

Reddy, J.N., 1993; *An Introduction to the Finite Element Method*, McGraw Hill.

Sinha, B.K., A.N. Norris and Shu-Kong Chang, 1994; *Borehole flexural modes in anisotropic formations*, Geophysics, 59(7), pp. 1037-1052.

Zoback, M.D. and M.L. Zoback, 1989 ; *Stress in the earth's lithosphere.*, Encyclopedia of Earth Sciences Series (R.W. Fairbridge, Series Ed.), Van Nostrand Reinhold Co., New York, 1221-1232.

Zoback, M.D., M. Daniel and L. Mastin, 1985; *Well Bore Breakouts and in Situ Stress*, Journal of Geophysical Research, 90(B7), pp 5523-5530.

Zoback, M.D., L. Mastin and C. Barton, 1986; *In-situ stress measurements in the deep boreholes using hydraulic fracturing, wellbore breakouts, and stonely wave polarization*, Proceedings of the International Symposium on Rock Stress and Rock Stress Measurements/Stockholm/1-3 September 1986, pp 289-299.

Zoback, M.D. and J. Townend, 2001; *Implications of hydrostatic pore pressures and high crustal strength for the deformation of intraplate lithosphere*, Tectonophysics, 336, pp 19-30.